PAPER • OPEN ACCESS

Optical absorption of composition-tunable InGaAs nanowire arrays

To cite this article: J Treu *et al* 2019 *Nanotechnology* **30** 495703

View the article online for updates and enhancements.

Recent citations

- Comparison of quantum and collection efficiency of fieldassisted uniformdoping and exponentialdoping GaN nanowire cathodes
  Feifei Lu *et al*

- Pulsed THz emission from wurtzite phase catalyst-free InAs nanowires
  R Adomaviius *et al*

Optical absorption of composition-tunable InGaAs nanowire arrays

J Treu, X Xu, K Ott, K Saller, G Abstreiter, J J Finley and G Koblmüller

Walter Schottky Institut, Physik Department & Center for Nanotechnology and Nanomaterials, Technische Universität München, Garching, D-85748, Germany

E-mail: Gregor.Koblmueller@wsi.tum.de

CrossMark

Abstract

InGaAs nanowire (NW) arrays have emerged as important active materials in future photovoltaic and photodetector applications, due to their excellent electronic properties and tunable band gap. Here, we report a systematic investigation of the optical absorption characteristics of composition-tunable vertical InGaAs NW arrays. Using finite-difference time-domain simulations we first study the effect of variable composition (Ga-molar fraction) and NW array geometry (NW diameter, period, fill factor) on the optical generation rate. NWs with typical diameters in the range of $\sim$100–250 nm lead to generation rates higher than the equivalent bulk case for moderate fill factors (NW period of $\sim$0.3–0.8 μm), while slightly smaller fill factors and increased diameters are required to maintain high generation rates at increased Ga-molar fraction. The optical absorption was further measured using spectrally resolved ultraviolet–visible-near-infrared (UV–vis-NIR) spectroscopy on NW arrays transferred to transparent substrates. Interestingly, large variations in Ga-molar fraction ($0 < x(\text{Ga}) < 0.5$) have a negligible influence, while minute changes in NW diameter of less than $\pm$20 nm affect the absorption spectra very strongly, leading to pronounced shifts in the peak absorption energies by more than $\sim$700 meV. These results clearly highlight the much larger sensitivity of the optical absorption behavior to geometric parameters rather than to variations in the electronic band gap of the underlying NW array.

Supplementary material for this article is available online

Keywords: III–V nanowire arrays, optical absorption, UV–vis-NIR spectroscopy

(Some figures may appear in colour only in the online journal)

1. Introduction

Semiconductor nanowire (NW) arrays have recently emerged as promising materials for next-generation photovoltaics and photodetection due to their distinct advantages over planar thin-film technologies [1–5]. In particular, NWs offer greater flexibility in combining different materials without conventional lattice mismatch restrictions, enabling integration on low-cost substrates (e.g. silicon) [4, 6, 7] while

simultaneously tuning the band gaps of the photoabsorbing material to the desired spectral regions [8, 9]. Also, NW arrays can absorb light at efficiencies larger than the equivalent bulk material due to enhanced light–matter interactions [2, 3, 10, 11]. These advantageous features have recently led to high-performance NW solar cells made from arrays of e.g. silicon [12] and III–V compound semiconductor NWs (e.g. GaAs(P), InP, InGaAs) [3, 13–16], where the employed material volume constituted only a small fraction of the equivalent thin-film case.

Amongst the III–V compound semiconductor materials, InGaAs NW arrays have particularly appealing properties for photovoltaic and photodetector applications. Firstly, InGaAs offers very high absorption coefficients (i.e. $\sim$up to

20× larger than that of Si, and few times larger than GaAs or InP), high carrier mobility, high responsivity and small dark currents, as recently observed in InGaAs NW-based photodetectors [17, 18]. Moreover, ternary InGaAs NWs offer large band gap tunability from the near-infrared (NIR) to the mid-infrared region ($0.35 < E_g < 1.42$ eV). This provides useful spectral regions for avalanche photodetectors in light detection and ranging systems [19], as well as the opportunity for broadband absorption of light over large portions of the solar spectrum [13]. Furthermore, InGaAs presents an important constituent in state-of-the-art multi-junction solar cells [20], and is expected to play a similar role in future NW solar cell designs due to the large degree of freedom in stacking different sub-cells in NW arrays [21].

Despite the prominent role that InGaAs NW arrays may play in future photoabsorption applications, the principles of their optical absorption characteristics have remained unexplored. In fact, the optical absorption has only been investigated at the limits of the binary constituents, GaAs and InAs NWs [22, 23], where mostly the role of geometrical parameters on the optical response was evaluated from ordered NW arrays. In contrast, the effects of composition and electronic band gap energy, which traditionally govern the optical absorption behavior in classical bulk-like material [24], have not yet been sufficiently investigated in NW arrays and, thus, present important metrics to be studied. In this respect, it is interesting to also explore what role the homogeneity (periodicity) of the NW array plays on the optical absorption under varying InGaAs composition. For example, recent work on non-periodic, randomly oriented ternary InGaN NW arrays with tunable composition revealed direct scaling of the optical absorption edge with composition [25], whereas theoretical work on high-periodicity NW arrays predict the material composition to play a minor role due to the metamaterial-like light–matter interactions in homogeneous NW arrays [26].

In this work, we therefore study the optical absorption characteristics of composition- and band gap tunable InGaAs NW arrays, and discriminate the effects of electronic band gap and geometrical parameters on the corresponding optical response. By providing both numerical simulations and experimental absorption spectroscopy, the absorption behavior in high-periodicity InGaAs NW arrays with composition tuned from $0 < x(\text{Ga}) < 1$ is investigated under variable fill factors and periods ($\sim$0.25 to $\sim$3 μm) as well as NW diameters ranging from $\sim$80 to 240 nm. Our results show unambiguously that the optical absorption is significantly governed by even miniscule changes in NW geometry, while alloy composition and electronic band gap play a negligible role.

2. Experimental details

All InGaAs NW arrays studied here were produced by selective area growth on Si (111) substrate using solid-source molecular beam epitaxy (MBE). Hereby, the Si (111) substrates were masked by a 20 nm thick SiO_2 layer where 1×1 cm^2 large lattices were pre-patterned with periodic

mask openings (80 nm diameter holes, and variable pitch of 0.25–2 μm) using nanoimprint lithography [7, 27, 28]. The InGaAs NW arrays were grown for 1 h in a completely catalyst-free process under highly As-rich conditions (beam equivalent pressure of 4.5×10^{-5} mbar) at temperatures of $\sim$500 °C–560 °C [27]. To tune the alloy composition (Ga-molar fraction) we adjusted the ratio between the Ga- and In-flux, while keeping the total group-III flux constant (i.e. 0.6 Å s^{-1}). The Ga-molar fraction of each NW array was directly determined from 2θ–ω scans in high-resolution x-ray diffraction [28]. Specifically, two sets of InGaAs NW samples with variable pitch ($p = 0.25\ \mu$m to $p = 2\ \mu$m) and variable alloy composition (tuned between $x(\text{Ga}) = 0$ (InAs) and $x(\text{Ga}) = 0.48$) were explored, as further described below.

To characterize the optical absorption unobscured by the underlying Si substrate, the NW arrays were transferred into a transparent polydimethylsiloxane (PDMS) membrane on a thin glass slide. Consequently, spectrally resolved measurements of the transmission and reflection were conducted at room temperature and in ambient by ultraviolet–visible–near-infrared (UV–Vis–NIR) spectroscopy using a PerkinElmar Lambda 900 UV–Vis–NIR spectrometer. Two broadband light sources (deuterium and halogen lamp) were used for the visible and infrared region (300–2800 nm) while detection was carried out using two grating monochromators together with a photomultiplier and lead sulfide detector. In transmission mode the NW array was mounted on a well-defined aperture and the transmitted light was collected over a large range of angles using an integrating Ulbricht sphere. Each measurement was calibrated using a blank sample without NWs, i.e. containing merely the PDMS membrane on glass. The PDMS membrane on glass has, as expected, very high optical transparency, with a transmission of >92% over the entire wavelength region of interest (see supplementary material available online at stacks.iop.org/NANO/30/495703/mmedia). For reflection measurements, the sample was mounted inside the integration sphere at a position opposite of the entry slit of the aperture. For both transmission and reflection measurements, the NW array was facing the incident beam to minimize the influence from the substrate.

3. Results and discussion

3.1. Finite-difference time-domain (FDTD) simulations

To first obtain a generalized picture about the optical absorption and its influence by both geometrical parameters and alloy composition, we performed numerical simulations for vertical, high-periodicity InGaAs NW arrays. Since typical InGaAs NWs have diameters much smaller than the illuminating wavelength [7, 13], the electromagnetic interaction within the ensemble of NWs cannot be neglected. As a result, simple effective medium theories [23] cannot be properly applied and a rigorous solution of Maxwell's equations is necessitated taking wave effects into account [29]. Therefore, we use the transfer matrix method and employ FDTD simulations (Lumerical Solutions, Inc.) when
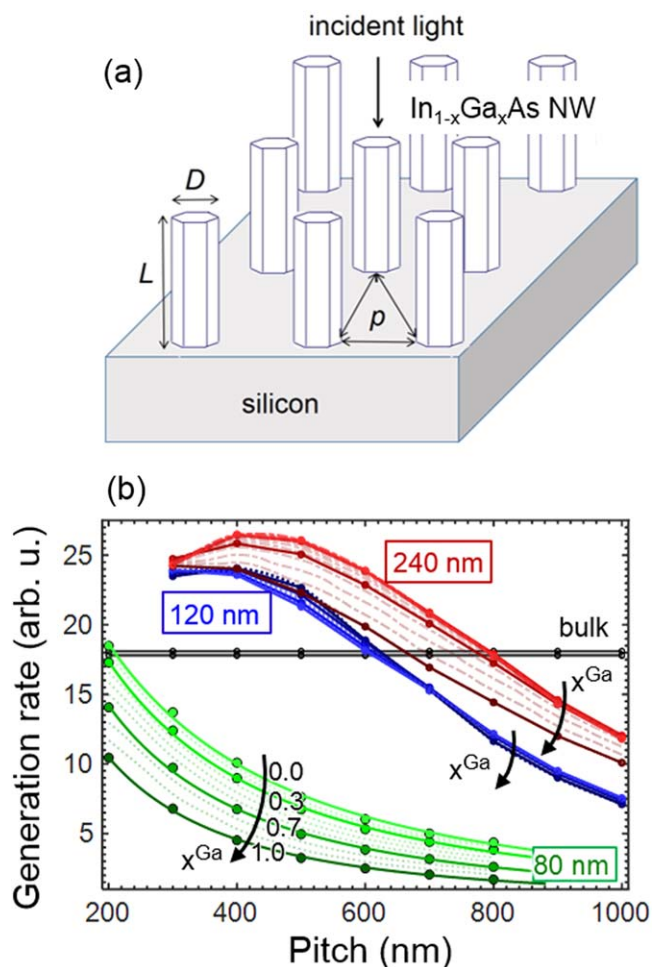
Figure 1. (a) Schematic drawing of the periodic InGaAs NW array on top of an infinitely thick Si substrate. The geometrical parameters are the NW length L and diameter D, and the period (pitch) p. A plane wave of light of wavelength 630 nm is incident normally onto the NW array. (b) Optical generation rate for 1 μm long InGaAs NWs with varying diameter D (80, 120, 240 nm) and Ga-molar fraction $[0 < x(\text{Ga}) < 1]$ plotted as a function of pitch. Simulated data are indicated by filled circles and interpolated curves as dashed lines. For comparison, the generation rate for a 1 μm thick planar InGaAs film (bulk) is shown also for variable $x(\text{Ga})$. Generation rates higher than the equivalent bulk material can be obtained at moderate pitch and NW diameters exceeding $\sim$100 nm.

dealing with such periodic structures. A schematic of the modeled high-periodicity InGaAs NW array is illustrated in figure 1(a). Hereby, we consider a triangular array of hexagonally shaped InGaAs NWs with length L, diameter D, and a pitch (period) p which is surrounded by air. For comparison, also a square lattice of the NW array was considered, but we found almost no difference in the absorption behavior by such change in symmetry (see supplementary material). The NW array is placed on top of an infinitely thick silicon (Si) substrate, containing a 20 nm thick SiO$_2$ mask layer, thereby representing state-of-the-art InGaAs NW arrays obtained by common selective area epitaxy (SAE) growth processes [7, 28, 30, 31]. As such our modeled structure is analogous to previous simulation studies [11, 26, 32], where the role of the underlying substrate plays only a minor role on the absorption

characteristics [32]. By applying periodic boundary conditions in-plane, the simulations are carried out within a unit cell to model the periodic structure. The simulation domain is closed in the growth direction with a perfectly matched layer to force impedance matching for minimal reflection. Light incident onto the NW array uses a plane wave, while a 3D-frequency-domain field monitor is employed near the top surface to collect data, and calculate the optical generation rate as a measure for the absorption behavior for different geometries and composition.

The generation rate denotes the number of charge carriers generated at each point of the device and can be calculated from the absorption per unit volume by integrating over the simulated spectrum of the NW volume. This requires detailed knowledge of the complex dielectric function ($\varepsilon = \varepsilon_1 + \text{i}\varepsilon_2$) of the respective material, both as a function of wavelength and composition. While the refractive indices and associated dielectric functions are well known for binary InAs, GaAs and InGaAs lattice matched to InP, only scarce information of the absorption coefficient over the entire InGaAs alloy compositional range is available in literature. Applying the so-called parametric semiconductor model [33], we follow Kim *et al* [34] to obtain the dielectric function for arbitrary composition by fitting and interpolating data obtained by spectroscopic ellipsometry. The results for both the real and imaginary part of the dielectric function in dependence of of Ga-molar fraction $x(\text{Ga})$ are shown in the supplementary material. Here, the data illustrates the expected trend that with increasing $x(\text{Ga})$ a decrease of the relative permittivity ε_2 and, thus, the extinction coefficient is observed.

Figure 1(b) shows the calculated optical generation rates for NW arrays with different diameters D and variable InGaAs composition, $x(\text{Ga})$, as a function of the pitch p under a fixed incident wavelength of $\sim$630 nm. To capture the most interesting parameter space, we focus on a pitch p varying from $\sim$0.2 to 1 μm and NW diameters from $\sim$80 to 240 nm (i.e. typical values of bottom-up InGaAs NWs [7, 13, 28, 30, 31]), which corresponds to an area fill factor of less than 0.15 of the equivalent planar material. For simplicity, we fixed the NW length to $L = 1$ μm, in line with the optimum lengths of NWs in high-performance NW solar cells [11]. In fact, when NWs are too long they do not gain in efficiency due to the limited absorption depth and correspondingly increased dark current density that scales directly with NW length [1]. Likewise, in axial NW p-n junctions the use of long NWs causes detrimental carrier recombination due to the limited minority carrier diffusion [3, 11].

The data in figure 1(b) highlights three important results that mimic closely recently observed trends in simulated InP-based NWs [11]. First, for comparatively small NW diameters of 80 nm (and less), we find that increasing fill factor (decreasing pitch) leads to a monotonic increase in the absorption (green data). This behavior resembles that of a classical ray optics description, where the maximum fraction of absorbed light is proportional to the surface coverage of the active material. Hence, in the limit of almost interconnected NWs, the generation rate reaches a maximum approaching the values obtained for bulk material. Note, the simulated data

follows an inverse quadratic relationship between absorbed light (generation rate g) and pitch, i.e. $gf(p) = a/(p + b)^2 \sim 1/p^2$, where a is a measure for the light absorbed per single NW at pitch p, and b accounts for the absorption when approaching the limit of interconnected NWs (i.e. fill factor $f \sim 1$). Changing the InGaAs alloy composition from InAs ($x(\text{Ga}) = 0$) to GaAs ($x(\text{Ga}) = 1$) decreases the generation rate by $\sim$2–3-fold, in compliance with a rise in band edge energy and, hence, lower extinction coefficient (i.e. $\kappa = 0.6$ (for $x(\text{Ga}) = 0$) and $\kappa = 0.23$ (for $x(\text{Ga}) = 1$) at a wavelength of 630 nm).

In contrast, the monotonic relationship between generation rate and pitch ceases to hold true for NW diameters of $D = 120$ and 240 nm, i.e. when the dimensions of the NWs approach the optical wavelengths such that NW-arrays are rather treated as metamaterials [26]. Clearly, at such increased NW diameters the generation rate exhibits a distinct maximum, where the absorption exceeds well the equivalent value for the bulk case even at moderate pitch ($\sim$0.3–0.5 μm), which corresponds to relatively small fill factors of $\sim$0.12–0.18. This observation is attributed to the pronounced resonant light trapping (intrinsic antireflection) effects found in periodic NW arrays with increased diameter and period [3, 11, 22, 26, 29, 35], where the incoupling efficiency of the incident light can be maximized. Specifically, we find that the generation rate increases with larger diameter NWs, however, too thick NWs are expected to corrupt the generation rate due to higher reflection at the top of the array and changes of the dispersion characteristics reducing the favorable absorption enhancement [11]. This is also accounted for by the decreased generation rate and the shift of the maximum absorption towards smaller pitches when the NW diameter is decreased from 240 to 120 nm (see figure 1(b)). Interestingly, changes in the Ga-molar fraction yield only very small changes in the generation rate for the large diameter NWs. To maintain maximum absorption at increased Ga-molar fraction requires, thus, only small changes in NW diameter and/or pitch, as noted by the small shifts in generation curves upon variations in composition. These observations suggest that the absorption characteristics are mainly influenced by the structure rather than the material composition.

3.2. Morphologies and optical colors of InGaAs NW arrays

To verify this and explore the influence of alloy composition and geometrical parameters on the optical absorption experimentally, we investigated two sets of MBE-grown InGaAs NW array samples. In particular, we explore (i) InGaAs NW arrays grown under a fixed pitch $p = 0.25$ μm with alloy composition tuned between $x(\text{Ga}) = 0$ (InAs) and $x(\text{Ga}) = 0.48$ (sample series A1–A4), and (ii) binary InAs NW arrays grown with variable pitch between $p = 0.25$ μm and $p = 2$ μm (sample series B1–B3), as further listed in table 1. Starting with the first series, figure 2(a) shows a representative scanning electron microscopy (SEM) image of an InGaAs NW array with a Ga-molar fraction of $x(\text{Ga}) = 0.28$ as grown on Si(111). Similar to recent state-of-the-art InGaAs NW arrays grown by SAE–MBE [7, 27, 28],

Table 1. Summary of the geometrical parameters (NW diameter, length, pitch, and fill factor) for the two sets of InGaAs NW arrays investigated, i.e. alloy composition series (A1–A4) and pitch series (B1–B3). The geometrical parameters were derived from statistical analysis of >20 NWs/sample using SEM.

Sample	$x(\text{Ga})$	Diameter D (nm)	Length L (μm)	Pitch p (μm)	Fill factor
A1	0	76 ($\pm$2)	2.39 ($\pm$0.21)	0.25	0.06
A2	0.11	79 ($\pm$7)	1.59 ($\pm$0.12)	0.25	0.07
A3	0.28	124 ($\pm$6)	0.94 ($\pm$0.09)	0.25	0.16
A4	0.48	116 ($\pm$4)	1.29 ($\pm$0.11)	0.25	0.14
B1	0	96 ($\pm$7)	2.15 ($\pm$0.27)	0.25	0.10
B2	0	114 ($\pm$5)	2.04 ($\pm$0.26)	0.50	0.03
B3	0	160 ($\pm$9)	4.80 ($\pm$0.30)	2.00	0.004

the array shows excellent periodicity with NWs being untapered and having hexagonal shape with sidewall facets delineated by {1–10} planes. In addition, NWs with low-to-intermediate Ga-molar fractions have a wurtzite (WZ) type crystal structure with a high frequency of stacking defects, while NWs with higher $x(\text{Ga}) > 0.4$ exhibit a heavily twinned zincblende (ZB) crystal structure [7, 28]. The range of alloy compositions investigated here corresponds to a variation in band gap energy from $\sim$0.45 eV ($x(\text{Ga}) = 0$, InAs) to $\sim$0.82 eV ($x(\text{Ga}) = 0.48$), as determined by micro-photoluminescence (μPL) spectroscopy [28, 36].

In figures 2(b)–(e) we show top-view SEM images of all four investigated InGaAs NW arrays with Ga-molar fractions of $x(\text{Ga}) = 0$ (b), $x(\text{Ga}) = 0.11$ (c), $x(\text{Ga}) = 0.28$ (d), and $x(\text{Ga}) = 0.48$ (e), confirming the excellent growth selectivity of NWs from the periodic mask openings. Note that we observe nearly perfect periodicity in NW arrays with increasing Ga- content, while pure InAs NWs (figure 2(b)) exhibit slightly inferior periodicity. This is mainly due to arbitrary nucleation from the edge of the mask openings in pure InAs NWs [37]. Even though all NW arrays were grown under identical conditions, the NW diameters and lengths vary slightly among the different samples, due to the nature of the catalyst-free growth mode [7, 27, 28]. As seen by the top-view SEM images, the NW diameter increases slightly from $\sim$80 nm (for In-rich InGaAs NWs) to around $\sim$120 nm (for more Ga-rich InGaAs NWs). From these data we further extracted the corresponding fill factors of each sample, which are on the order of $\sim$0.06–0.16 (as listed in table 1). Interestingly, photographic images taken from each NW array exhibit different optical colors in the visible spectrum, suggesting that each array absorbs light at a different wavelength. Tentatively, we suggest that the underlying metric governing the different light absorption behavior in these InGaAs NW arrays is either the change in alloy composition or, although small, the observed variation in NW diameter [38]. To discriminate the dominant effects leading to the different light absorption, spectrally resolved absorption measurements were performed as illustrated in the following.
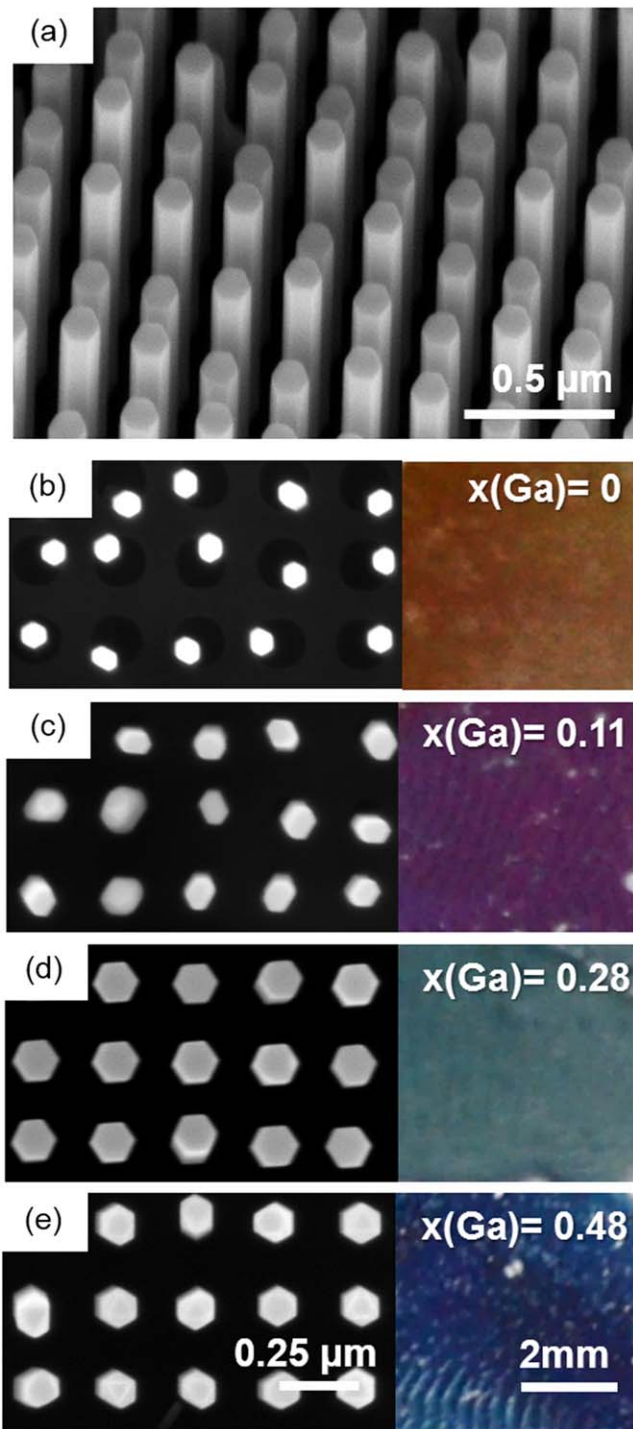
Figure 2. (a) Typical InGaAs NW array exemplified for $x(Ga) = 0.28$ as recorded by SEM imaging under a tilt angle of $70°$. (b)–(e) Top-view SEM images (left) and photographic images (right) images of composition-tuned InGaAs NW arrays with different Ga-molar fraction of (b) $x(Ga) = 0$, (c) $x(Ga) = 0.11$, (d) $x(Ga) = 0.28$, and (e) $x(Ga) = 0.48$. The scale bars shown in (e) are identical for all other images.

Figure 3. (a) Spectrally resolved transmittance T and reflectance R of an InGaAs NW array sample with $x(Ga) = 0.48$ as recorded by UV–Vis–NIR spectroscopy. The dip in the transmittance spectrum marked by the arrow features a resonant absorption near $\sim 2\,eV$. (b) Plot of the normalized absorption coefficient as a function of the incident photon energy for the four investigated InGaAs NW array samples with different Ga-molar fraction $x(Ga)$. The absorption peaks for each NW array are determined by the equivalent complementary color (see figures 2(b)–(e)), which is also used to label the spectra of the given NW arrays (i.e. red: $x(Ga) = 0$, purple: $x(Ga) = 0.11$, cyan: $x(Ga) = 0.28$, blue: $x(Ga) = 0.48$).

3.3. Optical absorption measurements

To realize comparable analysis of the optical absorption unaffected by the Si substrate, the corresponding NW arrays were transferred into a P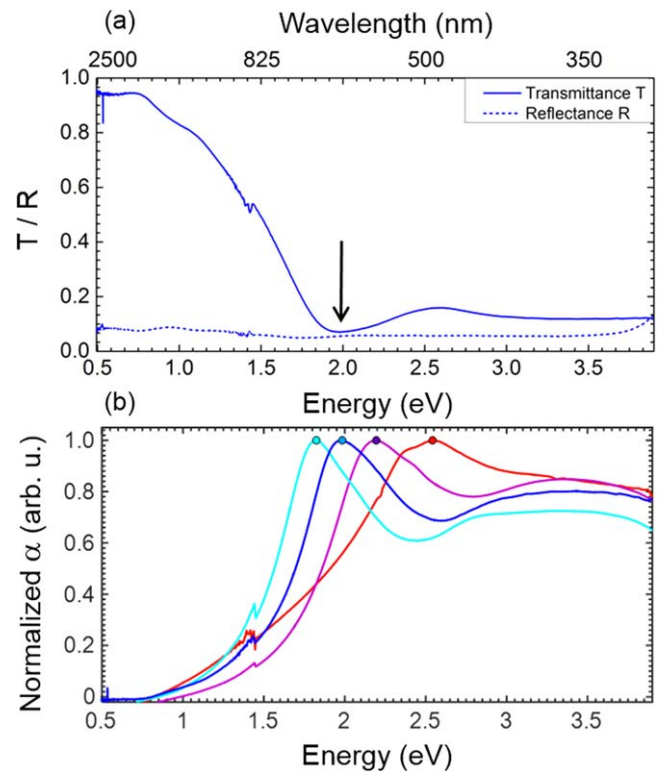DMS membrane on a thin glass slide and measured by UV–Vis–NIR absorption spectroscopy at room temperature. Figure 3(a) shows a typical set of transmission and reflection measurements of an InGaAs NW array in PDMS with $x(Ga) = 0.48$ (sample A4). At low energy the sample exhibits high transmittance of $T \sim 95\%$ (at $0.5\,eV$), followed by a monotonic decrease in transmittance down to below 10% towards higher photon energies. In contrast, the reflectance remains approximately constant near $R \sim 6$ (± 1)% over the entire spectral region. Thus, in the low-frequency regime the much higher transmittance cannot be compensated by the low reflectance, leading to insufficient absorption of low-energy photons in the NW structure. In contrast, in the high-frequency regime entering the visible spectral range ($> 2\,eV$), where both transmittance and reflectance are very low, the absorptance A [$A(\lambda) = 1 - T(\lambda) - R(\lambda)$] is consequently increased to more than 85%. Given the non-absorbing nature of the PDMS matrix and the very small fill factor (0.14) of the NW array, this indicates that the sparsely arranged NWs absorb light in the visible very efficiently. This confirms the widely observed absorption enhancements in NW arrays [3, 10, 11, 23, 26, 29], which are a result of the much larger absorption cross-sections than the geometric
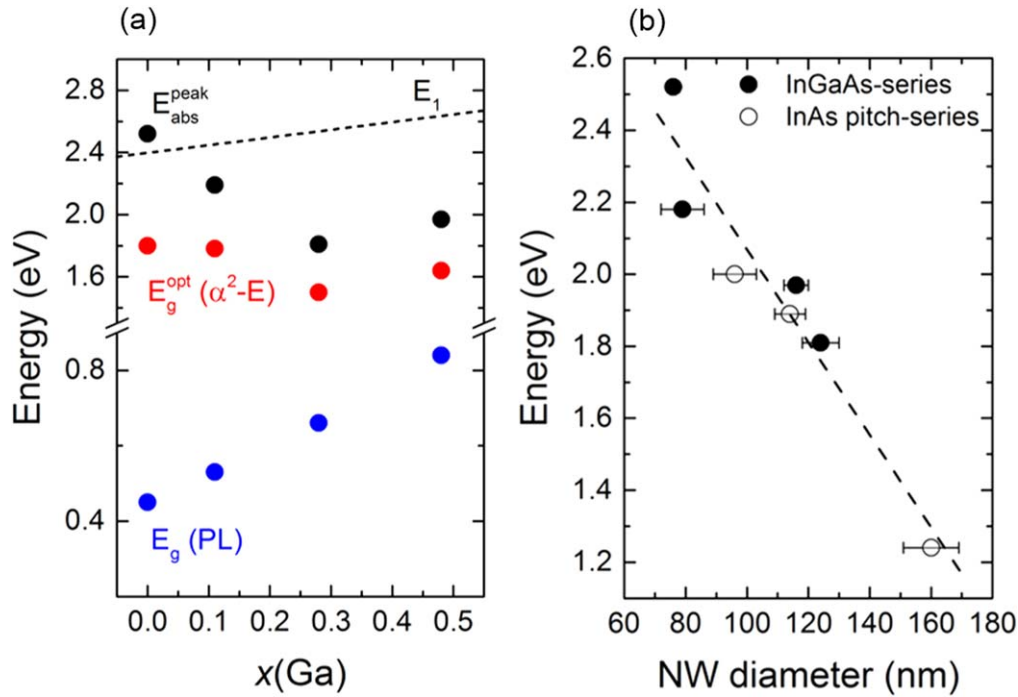
Figure 4. (a) Evolution of the optical band gap energy ($E_g{}^{opt}$, red data, extracted from α^2–E plots) in comparison to the peak absorption energy (black data) and the direct band gap energy (E_g, blue data, adapted from PL measurements of [28, 36]). The dashed line indicates the $E_1(A)$ band gap energy. (b) Peak absorption energy as a function of NW diameter as obtained from two different sample series. The InGaAs NW-series (closed symbols) exhibits datapoints derived from figure 3, while the InAs NW pitch-series (open symbols) refers to datapoints extracted from figure 5. The dashed line represents a best linear fit to the data.

cross-section when NWs have sub-wavelength dimensions [39]. Furthermore, the transmission spectrum exhibits a characteristic minimum (dip) at around 2 eV (marked by the arrow), which in turn leads to a distinct peak in the absorption as clearly seen in figure 3(b). This feature evidences an energy-selective resonant absorption behavior of the NW array, as was also found in highly ordered NW arrays of various other materials systems [23, 29, 38, 40, 41]. The origin of the resonant absorption stems from the wavelength-selective coupling and field distribution of the guided modes supported by each NW [38, 41]. Since we only observe one major spectral dip (peak) in the transmission (absorption) data, only the fundamental mode is expected to be relevant in this process [38].

To further illustrate the wavelength-selective resonant absorption behavior, we plot in figure 3(b) the normalized absorption coefficient α for all four investigated InGaAs NW arrays as a function of the incident photon energy. We chose this representation since from the square dependence of α (i.e. α^2–E) we can further extract the optical band gap energy (see figure 4(a) and supplementary material). The absorption coefficient α was derived from the relationship $\alpha = 1/d \cdot \log (T/1{-}R)$ [42], where T and R are the spectrally resolved data for the transmittance and reflectance, and d is the sample thickness. Since we deal here with a NW/PDMS composite material, we describe d by the equivalent thickness $d = fL$, in which f is the fill factor and L is the average length of the NW, an approximation which holds true for highly diluted media in the framework of Lambert–Beer's law [43].

The data obtained from each sample shows very similar spectral characteristics, i.e. a single pronounced absorption peak in the visible spectral range, which shifts in energy, i.e. between $1.8\,\mathrm{eV} < E_{\mathrm{abs}} < 2.5\,\mathrm{eV}$, depending on the sample. Note that there is a direct relationship between the spectral position of the absorption peak and the corresponding color observed in the photographic image of figures 2(b)–(e). In particular, the observed colors are the equivalent complementary colors to the wavelengths that are absorbed stronger, meaning that the NW arrays act as efficient color filters in the visible spectral range [38]. To emphasize this, we labeled the spectrum of each sample by the equivalent complementary color for the given wavelength of the absorption peak. We further note that the absorption peak becomes more pronounced towards longer wavelengths. This can be attributed to a change in refractive index contrast of the NW/ PDMS composite with increasing wavelength [38]. However, we also suggest that the periodic nature of the NW array has a strong influence, since the formation of a distinct absorption peak is absent in the case of random, non-periodic NWs (see supplementary material). Interestingly, the absorption spectra tend to shift towards lower energy with increasing Ga-molar fraction, except for sample A4 which is blue-shifted despite its largest $x(\mathrm{Ga})$. Considering the expected increase in band gap energy (E_g) with rising $x(\mathrm{Ga})$, the observed shifts are, thus, not intuitive from an electronic standpoint of view.

To identify correlations between the shifts in the absorption spectra and the specific band gap energy of the respective InGaAs NW arrays, figure 4(a) plots the peak absorption energies as a function of $x(\mathrm{Ga})$ (black data). In
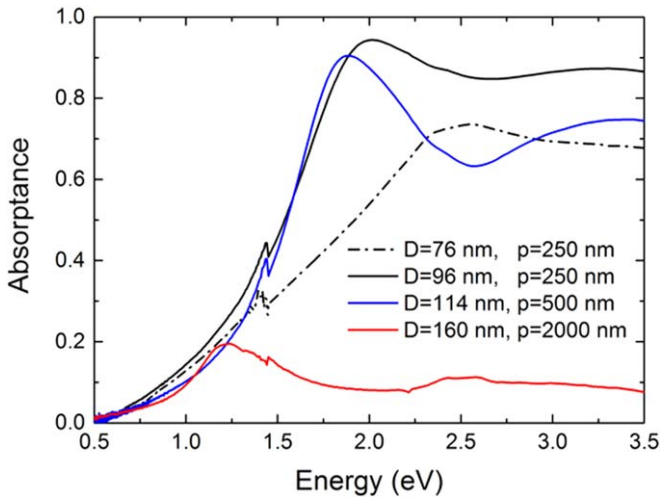
Figure 5. (a) Absorption spectra of the InAs NW pitch-series (samples B1–B3, A1) as recorded by UV/Vis/NIR absorption spectroscopy. Maximum absorptance is observed for intermediate NW diameters and moderate NW spacing, while the peak absorption shifts to lower photon energies with increasing NW diameter.

addition, we also show the optical band gap energies (E_g^{opt}, red data) as extracted from linear fits of the α^2–E dependency (see supplementary material). The optical band gap energy in these NW arrays is expected to be dominated by three major factors, i.e. the direct band gap of the ternary material (E_g, blue data, estimated from previous PL measurements [27, 36]), the $E_1(A)$ band gap where the highest amount of joint-density of states is located at, and geometrical parameters that govern the coupling of incident light into the NW waveguide modes. Comparison with the direct band gap energies E_g shows that the measured optical band gap energies show neither similar order of magnitude nor do they follow the same monotonic increase with x(Ga). The much higher values of E_g^{opt} might be explained by the fact that in the absorption measurements the interband transition is not only occurring via the energetically lowest direct band gap transition (at the Γ-point) but also via the high-energy $E_1(A)$ transition. Still, the $E_1(A)$ gap increases continually with increasing x(Ga), i.e. from $\sim$2.4 eV (InAs) [44] to $\sim$2.9 eV (GaAs) [45] (see dashed line), which can thus not fully describe the observed decrease of the optical band gap with rising x(Ga). Besides the absent correlation with alloy composition, the data can also not capture any changes in crystal structure since the variations between the ZB and WZ-phase InGaAs band gap are very small (i.e. few tens of meV [36]). This clearly hints to the fact that most likely the geometrical factors of the NW array obscure the evaluation of band structure properties from absorption measurements.

To account for the geometrical parameters, figure 4(b) plots therefore the peak absorption energy data as a function of the NW diameter D. The datapoints shown here comprise two sets of experimental data, i.e. from the absorption measurements shown in figure 3 (InGaAs alloy composition series, closed symbols) and those illustrated in figure 5 below (InAs NW pitch series, open symbols). We find a linearly decreasing peak absorption energy with increasing NW

diameter, in analogy to previous reports on Si NW arrays [38]. In particular, an increase in NW diameter from $\sim$80 nm up to $\sim$160 nm results in a strong red-shift in the peak absorption energy by as much as $\sim$1.3 eV. Moreover, the fact that data from both sample series fit fairly well onto the universal linear dependency illustrates that the absorption characteristics are largely insensitive to the alloy composition, while strongly dominated by the NW diameter.

Given the obvious sensitivity to geometrical parameters, we further describe in the following how the absorption behavior is not only influenced by NW diameter but also by the fill factor (pitch p) of the NW array. In this case, we focus therefore on pure binary InAs NWs fabricated with variable pitch (0.25–2 μm) (sample series B1–B3) grown under otherwise similar growth conditions as the InGaAs NW composition series. Corresponding SEM images of these NW arrays are shown in the supplementary material. Due to the large variation in pitch, InAs NWs grown under the catalyst-free growth mode exhibit an increased NW diameter for larger pitches (e.g. $\sim$160 nm for 2 μm pitch) in comparison to smaller pitches (e.g. $\sim$96 nm for 0.25 μm pitch, $\sim$114 nm for 0.5 μm pitch, respectively). This observation is well known and ascribed to the surface diffusion-limited growth kinetics during selective area epitaxial growth processes [37].

Figure 5 shows the corresponding absorption spectra of the four different InAs NW arrays, where three important results are directly revealed. First, the peak absorption shifts continually to smaller photon energies with increasing NW diameter, in line with the data and discussion provided in figures 3 and 4. Secondly, under constant pitch of $p = 0.25$ μm a slight increase in NW diameter from $\sim$76 nm to $\sim$96 nm results in a substantial increase in the absorptance in the high-frequency regime, despite similar NW length. This behavior mimics closely the simulated data of figure 1 and confirms that incident light couples more efficiently into NWs of wider diameter [11], even though the intrinsic absorption coefficient of InAs tends to decrease towards longer wavelength [46]. Thirdly, increasing the pitch from 0.25 μm to $\sim$0.5 μm, which corresponds to a significant decrease in fill factor from $\sim$0.1 to $\sim$0.03 does not alter the maximum absorptance. This confirms that even for more sparsely arranged NWs enhanced absorption can be maintained. The data also verifies that a slightly increased NW diameter requires a higher pitch for maximum absorption to be observed, in line with the simulated data of figure 1. Finally, as expected from simulations (see figure 1 and [11, 26]), a more drastic decrease in fill factor by one additional order of magnitude leads to a rapid drop in absorption (sample B3). Under such large wire-to-wire separation we only observe a peak absorptance of only $\sim$20%, even though the NW diameter and the NW length were further increased in this particular array. These trends therefore clearly evidence that the absorption in InGaAs NW arrays is strongly governed by geometrical parameters, showing that intermediate NW diameters as well as certain sparsity with moderate fill factors are necessary to obtain optimum absorption characteristics.

4. Conclusions

In summary, we investigated the optical absorption characteristics of composition-tuned, periodic InGaAs NW arrays by numerical simulations and absorption spectroscopy measurements. Our results directly evidence that tuning the alloy composition of the InGaAs NW arrays has negligible effect on the optical absorption behavior. In contrast, quite small changes in the geometrical parameters, i.e. NW diameter, affect the absorption spectra very strongly leading to pronounced absorption peak shifts from the visible to the near-IR spectral range consistent with the observation of different optical colors of the NW arrays. We further explored the dependencies of the maximum absorptance on NW diameter and fill factor, and found optimum absorption for NW diameters in excess of 100 nm at moderate NW spacing of $\sim$0.3–0.6 μm. Departure from the distinct periodicity of the NW array weakens the absorption behavior without the observation of resonant absorption peaks. These findings are expected to enable useful guidelines in the construction and optimization of ternary and multi-component NW-array solar cells and array-type photodetectors.

Acknowledgments

ORCID iDs

X Xu https://orcid.org/0000-0003-2175-2300
G Koblmüller https://orcid.org/0000-0002-7228-0158

References

[1] Kayes B M, Atwater H A and Lewis N S 2005 *J. Appl. Phys.* **97** 114302
[2] Garnett E and Yang P 2010 *Nano Lett.* **10** 1082
[3] Wallentin J *et al* 2013 *Science* **339** 1057
[4] Wei W, Bao X-Y, Soci C, Ding Y, Wang Z-L and Wang D 2009 *Nano Lett.* **9** 2926
[5] Leung Y H, He Z B, Luo L B, Tsang C H A, Wong N B, Zhang W J and Lee S T 2010 *Appl. Phys. Lett.* **96** 053102
[6] Mårtensson T, Svensson C P T, Wacaser B A, Larsson M W, Seifert W, Deppert K, Gustafsson A, Wallenberg L R and Samuelson L 2004 *Nano Lett.* **4** 1987
[7] Koblmüller G and Abstreiter G 2014 *Phys. Stat. Sol.—RRL* **8** 11
[8] Wen L, Li X, Zhao Z, Bu S, Zeng X S, Huang J-H and Wang Y 2012 *Nanotechnology* **23** 505202
[9] Chen Y, Pistol M E and Anttu N 2016 *Sci. Rep.* **6** 32349
[10] Garnett E C, Brongersma M L, Cui Y and McGehee M D 2011 *Annu. Rev. Mater. Res.* **41** 269
[11] Kupec J, Stoop R L and Witzigmann B 2010 *Opt. Express* **26** 27589
[12] Kumar D, Srivastava S K, Singh P K, Husain M and Kumar V 2011 *Sol. Energy Mater. Sol. Cells* **95** 215
[13] Shin J C, Kim K H, Yu K J, Hu H, Yin L, Ning C-Z, Rogers J A, Zuo J-M and Li X 2011 *Nano Lett.* **11** 4831
[14] Cui Y *et al* 2013 *Nano Lett.* **13** 4113
[15] Holm J V, Jorgensen H I, Krogstrup P, Nygård J, Liu H and Aagesen M 2013 *Nat. Commun.* **4** 1498
[16] Åberg I *et al* 2016 *IEEE J. Photovolt.* **6** 185
[17] Senanayake P, Hung C-H, Shapiro J, Lin A, Liang B, Williams B S and Huffaker D L 2011 *Nano Lett.* **11** 5279
[18] Tan H *et al* 2016 *Nano-Micro Lett.* **8** 29
[19] Farrell A C, Meng X, Ren D, Kim H, Senanayake P, Hsieh N Y, Rong Z, Chang T-Y, Azizur-Rahman K M and Huffaker D L 2019 *Nano Lett.* **19** 582
[20] Dimroth F *et al* 2014 *Prog. Photovolt.: Res. Appl.* **22** 277
[21] Popescu B, Popescu D, Luppina P, Treu J, Koblmüller G, Lugli P and Goodnick S M 2015 *IEEE Int. Conf. Nanotechnol. Proc.* pp 728–31
[22] Guo H, Wen L, Li X, Zhao Z and Wang Y 2011 *Nanoscale Res. Lett.* **6** 617
[23] Wu P M, Anttu N, Xu H Q, Samuelson L and Pistol M-E 2012 *Nano Lett.* **2** 1990
[24] Vurgaftman I, Meyer J R and Ram-Mohan L R 2001 *J. Appl. Phys.* **89** 5815
[25] Kuykendall T, Ulrich P, Aloni S and Yang P 2007 *Nat. Mater.* **6** 951
[26] Kupec J and Witzigmann B 2009 *Opt. Express* **17** 10399
[27] Treu J, Speckbacher M, Saller K, Morkötter S, Döblinger M, Xu X, Riedl H, Abstreiter G, Finley J J and Koblmüller G 2016 *Appl. Phys. Lett.* **108** 053110
[28] Hertenberger S *et al* 2012 *Appl. Phys. Lett.* **101** 043116
[29] Hu L and Chen G 2007 *Nano Lett.* **7** 3249
[30] Tomioka K, Tanaka T, Hara S, Hiruma K and Fukui T 2011 *IEEE J. Select. Top. Quant. Electron* **17** 1112
[31] Scofield A C, Kim S-H, Shapiro J N, Lin A, Liang B, Scherer A and Huffaker D L 2011 *Nano Lett.* **11** 5387
[32] Fountaine K T, Cheng W-H, Bukowsky C R and Atwater H A 2016 *ACS Photonics* **3** 1826
[33] Johs B, Herzinger C M, Dinan J J, Cornfeld A and Benson J D 1998 *Thin Sol. Films* **313–314** 137
[34] Kim T J, Ghong T H, Kim Y D, Kim S J, Aspnes D E, Mori T, Yao T and Koo B H 2003 *Phys. Rev.* B **68** 115323
[35] Anttu N and Xu H Q 2013 *Opt. Express* **21** A558
[36] Morkötter S *et al* 2013 *Phys. Rev.* B **87** 205303
[37] Hertenberger S, Rudolph D, Bichler M, Finley J J, Abstreiter G and Koblmüller G 2010 *J. Appl. Phys.* **108** 114316
[38] Seo K, Wober M, Steinvurzel P, Schonbrun E, Dan Y, Ellenbogen T and Crozier K B 2011 *Nano Lett.* **11** 1851
[39] Kattawar G W and Einser M 1970 *Appl. Opt.* **9** 2685
[40] Bao H and Ruan X 2010 *Opt. Lett.* **35** 3378
[41] Cao L, Fan P, Vasudev A P, White J S, Yu Z, Cai W, Schuller J A, Fan S and Brongersma M L 2010 *Nano Lett.* **10** 439
[42] Bass M, DeCusatis C, Enoch J, Lakshminarayanan V, Li G, MacDonald C, Mahaja V and Van Stryland E 2009 *Handbook of Optics, 3rd IV: Optical Properties of Materials, Nonlinear Optics* (New York: McGraw-Hill)
[43] Ceroni P 2011 *The Exploration of Supramolecular Systems and Nanostructures by Photochemical Techniques* (Berlin: Springer)
[44] Zardo I, Yazji S, Hörmann N, Hertenberger S, Funk S, Mangialardo S, Morkötter S, Koblmüller G, Postorino P and Abstreiter G 2013 *Nano Lett.* **13** 3011
[45] Wang C S and Klein B M 1981 *Phys. Rev.* B **24** 3417
[46] Aspnes D E and Studna A A 1983 *Phys. Rev.* B **27** 985